Electrochemical Characterization of Different Layers of Composite Incorporated Hot-Dip Zinc Coating

S.R. Arunima[1,2,*]

[1]Department of Chemistry, University of Kerala, Kariavattom Campus, Thiruvananthapuram-695581, India
[2]Department of Chemistry, Sree Narayana College for Women, Kollam-691001, India

*Corresponding author: E-mail: arunimasasidharan@gmail.com

The present study beneficially explores nano TiO_2 incorporated hot-dip zinc coatings for the enhanced corrosion protection of steel. Various electrochemical analyses such as open circuit potential (OCP), electrochemical impedance spectroscopy (EIS) and potentiodynamic polarization studies were adopted to evaluate the enhanced galvanic performance and the stability of nano TiO_2 composite incorporated coatings. The low corrosion current density and high polarization resistance of tuned composition of TiO_2 incorporated hot-dip zinc coatings confirm its enhanced galvanic and corrosion resistant properties. The enhanced performance of TiO_2 incorporated zinc coating was attributed to the combined effect of barrier and sacrificial behaviours.

Keywords: Corrosion, Zinc coating, Impedance, Polarization, Barrier protection.

INTRODUCTION

Steel of different forms is an integral part of building and construction industry due to its high strength, durability and relative inexpensiveness compared to other more exotic materials. However, the major drawback of steel is its natural tendency to undergo corrosion in humid atmosphere. Corrosion is the deterioration of materials by chemical interaction with their environment. Steel has been a frequent choice of engineering materials in today's economy for various construction/manufacturing industries, its protection from corrosion needs great importance. Hot-dip galvanization process offers a unique combination of superior properties such as high strength, formability, light weight, corrosion resistance, low cost and recyclability. Hot-dip galvanized steels have been extensively used in industrial fields such as automobiles, electrical home appliances or construction due to their excellent corrosion resistance characteristics [1]. The reason for the extensive use of hot-dip galvanization is the two-fold protective nature of the coating. As a barrier coating, it provides a tough, metallurgically bonded zinc coating that completely covers the steel surface and protects steel from corrosion. Additionally, the sacrificial action of zinc protects the steel even when damage or a minor discontinuity occurs on its surface.

During hot-dip galvanization process, a metallurgical reaction taking place between Fe and Zn, which resulted the formation of a heterogeneous assembly of different phases composed of mainly Fe and Zn [2]. After solidification, the coating consists of an outer layer of 100 wt.% zinc (η layer) and inner layers called alloy layers consisting of intermetallic phases of iron and zinc such as zeta (ζ) layer (94 wt.% Zn-6 wt.% Fe), delta (δ) layer 90 wt.% Zn-10 wt.% Fe) and gamma (γ) layer (75 wt.% Zn-25 wt.% Fe). The galvanic efficiency of hot-dip zinc coating depends on the alloy formation of outer layer and also the composition of inner alloy layers at the coating substrate interface [3]. These intermetallic layers are relatively harder than the underlying steel and provide exceptional protection against coating damage. The presence of metal oxides in the inner layers can modify the Fe-Zn alloy phases and also enhances the sacrificial action of zinc; thereby, the metal underneath is protected. The use of nano ZnO, CeO_2, Al_2O_3, ZrO_2, Fe_2O_3 and different mixed oxides were widely used in hot-dip zinc coating [4-9]. These oxides have certain special properties such as antibacterial property, photocatalysis,

wear resistance, plasticity, corrosion resistance, *etc*. which can be well utilized for tuning hybrid zinc coating for precise applications.

The objective of the coating was designed in the view of achieving excellent performance of composite coatings. The present study focuses on the synthesis and characterization of nano TiO_2 and its effective incorporation into molten zinc bath for developing high performance hot-dip zinc coatings. This work explores the role of TiO_2, an effective ceramic material having non-toxicity and high stability and different inter-metallic layers on corrosion protection efficacy of hot-dip zinc coatings.

EXPERIMENTAL

Preparation and characterization of TiO_2 composite: The nano TiO_2 prepared by the thermal decomposition of $TiCl_4$. Required amount of $TiCl_4$ was dissolved in isopropanol having definite concentration. In order to homogenize, mixture was kept at room temperature for 4-5 h with constant stirring and then evaporated to dryness in a china dish followed by heating at 120 ℃ for 1 h in an oven. The resulting powder was then grinded using mortar and heated at 450 ℃ in a controlled muffle furnace for 1 h for the complete conversion of $TiCl_4$ to their corresponding oxide.

The crystallographic analysis of the composite was characterized using Philips X' Pert MPD X-ray powder diffractometer (Cu*K*α radiation λ = 1.540 Å at a voltage of 40 kV and a current of 30 mA in the 2θ range from 20 to 80º, at a scan rate of 2º per minute at a step size of 0.02º). The optical properties were analyzed using UV-visible diffused reflectance spectroscopy (Shimadzu UV-2450 analyzer). The vibrational modes of TiO_2 were studied using Shimadzu FTIR spectrometer in the mid IR range from 350 to 4000 cm^{-1} with KBr pellets. The surface morphological analysis and elemental composition of the composite was carried out using scanning electron microscope attached with EDAX instrument [NOVA Nano SEM 450].

Development and characterization of TiO_2 composite incorporated hot-dip zinc coatings: Mild steel (with Bureau of Indian Standard designation CR2 SPD; TATA Steel Ltd.) coupons of 3.5 cm × 2.5 cm × 0.1 cm dimension having composition C-0.09, Mn-0.34, P-0.04, S- 0.01, Si-0.05, Al-0.03 and Fe-99.44 (in wt.%) were polished with different grades of emery paper. The coupons were subsequently degreased using 5 wt.% NaOH, washed with distilled water and pickled in 8 wt.% HCl at room temperature to ensure that the surface of the coupons was free from any superficial oxide layer. Afterwards, the coupons were fluxed with 30 wt.% NH_4Cl solution and dried at 120 ℃ to avoid further oxidation of the surface and to enhance the adhesion of molten zinc to mild steel surface. After fluxing, the mild steel coupons were immersed into the molten Zn ingot (Binani zinc corporation assay 99.99%) at 450 ± 10 ℃ and kept for a period of 10-15 s, slowly withdrawn from the bath and the excess zinc was removed by hot air blowing [10]. The process parameters were fixed based on our preliminary studies performed under varying experimental conditions.

The crucible containing molten zinc along with different compositions of the nanoparticles was used for the development of TiO_2 incorporated hot-dip zinc coatings. The required quantity of TiO_2 (0.1, 0.2 and 0.5 wt.%) was added into the molten zinc bath and stirred well using a silicon carbide rod. The developed coatings were named as Zn-0.1 TiO_2, Zn-0.2 TiO_2 and Zn-0.5 TiO_2, respectively.

Electrochemical impedance studies and potentiodynamic polarization behaviour of hot-dip galvanized coatings were carried out using biologic science instruments, SP 200 (with EC-Lab software version 10.38). The analysis was carried out in 3.5 wt % NaCl as electrolyte, Ag/AgCl, satd. KCl, platinum mesh and the coating having 1 cm^2 exposed area were used as reference, counter and working electrodes, respectively. EIS studies were made over frequencies ranging from 2 MHz to 100 Hz *versus* OCP. Tafel polarization measurements were measured at a scan rate of 50 mV/s within the range from -2.0 to 0.5 V *versus* OCP. The effective incorporation and crystalline nature of TiO_2 nanoparticles incorporated hot-dip zinc coatings were analyzed using XRD. Morphological characteristics of the coatings were analyzed using SEM. The elemental composition was obtained using EDAX.

Layer-wise characterization of TiO_2 composite incorporated hot-dip zinc coating: Anodic dissolution of hot-dip zinc coatings was carried out in 3.5 wt.% NaCl solution by impressing anodic current densities of 10 mA/cm^2 for 1 h. Platinum mesh, SCE and hot-dip zinc coatings with unit exposed area were used as the counter electrode, reference electrode and working electrode, respectively. A Luggin probe-salt bridge was used to minimize the ohmic resistance. During dissolution the variation in potential with time was measured. Layer-wise galvanic performance was measured by using potentiodynamic polarization studies and electrochemical impedance spectroscopy (EIS).

RESULTS AND DISCUSSION

Phase and crystallinity of TiO_2 composite: The crystallographic structure of as-prepared TiO_2 composite had been confirmed using XRD patterns. The XRD pattern of TiO_2 composite prepared by thermal decomposition method is shown in Fig. 1A. The sharp peaks at 2θ = 25.5º, 38.6º, 53.9º, 55.3º, 62.8º, 68.9º and 75.1° were clearly evident from the XRD pattern. The peaks appeared at these 2θ values corresponds to the crystal planes of (101), (004), (105), (211), (204), (116) and (215), which indicated the formation of anatase TiO_2 (JCPDS 21-1272 [11-14]. The above planes of TiO_2 were assigned to tetragonal anatase TiO_2 [15,16]. It was clear from the XRD pattern that most of the strong diffraction peaks observed were characteristics of anatase TiO_2, which revealed that the synthesized composite was typical anatase titania with tetragonal crystal structure. The sharp peaks and the absence of unidentified peaks confirmed the crystallinity and high purity of the synthesized TiO_2 particles. From the X-ray diffraction results, the crystallite size of synthesized TiO_2 composite was calculated from the width of the peaks using Scherrer′s equation [17]. The average crystallite size was found to be 25-40 nm.

Structure and bonding characteristics of TiO_2 composite: The UV-visible absorption spectrum of as-prepared nano TiO_2 composite is shown in Fig. 1B. An absorption band around 385 nm was observed for the prepared TiO_2 composite. This may be attributed to the charge transfer between O^{2-} and Ti^{4+} with respect to the excitation of electrons from valence band
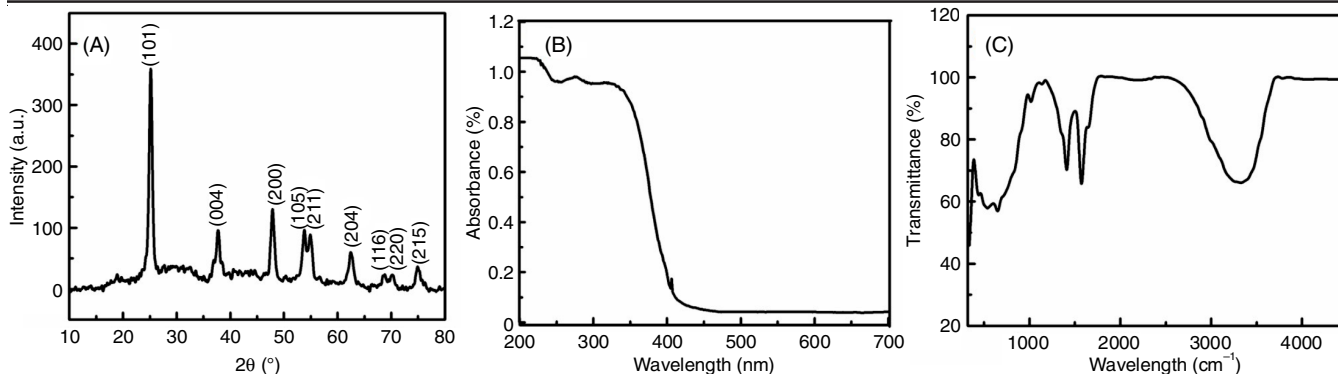
Fig. 1. (A) XRD pattern, (B) UV-visible and (C) FTIR spectrum of the synthesized TiO_2 composite

to conduction band [18]. The observed UV spectrum was in good agreement with those reported by Hung *et al.* [19] for nano TiO_2. According to Yang *et al.* [15], the wide absorption below 400 nm resulted from the band transition of TiO_2 related to its band energy of 3.2 eV. It has been reported that the absorption bands of anatase TiO_2 was located at about 383-400 nm [20]. These results also evidenced that synthesized TiO_2 composite was in anatase phase.

The FTIR spectrum of TiO_2 composite was measured in the range of 4000-400 cm^{-1} is presented in Fig. 1C. The strong band in the range of 700-500 cm^{-1} was associated with the characteristic modes of Ti-O stretching vibration of TiO_2 composite [14]. The presence of weak bands at 436 and 700 cm^{-1} accounts for the Ti-O-Ti bending and stretching modes of crystalline TiO_2, respectively [21]. The absorption range observed around 3400 and 1630 cm^{-1} could be related to the stretching and bending modes of hydroxyl groups of molecular water absorbed from atmosphere [14]. It has been reported in the literature [22] that the broad band obtained at 3500-3420 cm^{-1} was attributed to the hydroxyl groups on different sites and to the varying interactions between hydroxyl groups on TiO_2. The absence of bands in the range of 2900 cm^{-1} could be attributed to the complete removal of organic solvents that were used for the synthesis of TiO_2.

Morphological and compositional analysis of TiO_2 composite: The SEM images of nano TiO_2 particles at different magnifications are shown in Fig. 2A$_1$ and 2A$_2$. It was clear that the particles were spherical in shape with small facets and has narrow size distribution. The SEM images also revealed that the crystallites were in nanometer size with uniform morphology. The particles were of a regular shape and the boundaries between the particles were clearly visible from the images

(Fig. 2A$_1$ and 2A$_2$). Zhang *et al.* [23] reported that a good dispersion of small particles could provide more reactive sites for the reactants than agglomerated particle.

Fig. 2B shows the EDAX spectrum of as synthesized nano TiO_2 composite. The EDAX pattern indicated that titanium and oxygen were the major elements in the composite. There were no impurity peaks observed in the EDAX spectrum, which confirmed that the synthesized composite was in pure form.

Electrochemical evaluation of the developed coatings

Long term stability of hot-dip zinc coatings: The long-term stability of hot-dip zinc coatings in 3.5 wt.% NaCl solution was studied by continuously monitoring the open circuit potential (OCP). The variation in OCP of pure and nano TiO_2 incorporated hot-dip zinc coatings was monitored as a function of time after immersing in stagnant 3.5 wt.% NaCl solution for 30 days (Fig. 3A).

During initial days of exposure, all the coatings exhibited a steady and high negative OCP values in the range of -1.05 to -1.09 V. This was attributed to the sacrificial action of η phase by protecting the Fe-Zn intermetallic layers from corrosion during the course of exposure. As the time of exposure increases, the dissolution rate increases and the OCP values of coatings shifted to more anodic region. After 12 days of exposure, a significant shift in potential was observed in the case of pure zinc coating. But the composite incorporated coatings showed a steady change and a significant potential shift was observed only after 15 days. This was due to the fact that a protective barrier layer formed as a result of composite incorporation minimizes the dissolution of zinc in nano TiO_2 incorporated coatings during the course of exposure. During prolonged exposure in the electrolyte, the pure zinc coating exhibited a
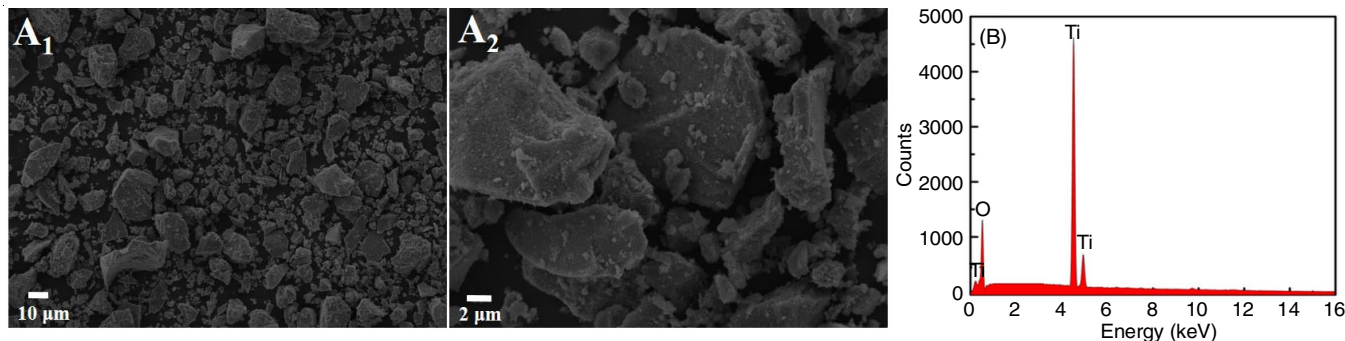
Fig. 2. (A$_1$) & (A$_2$) SEM images at magnifications 1 KX and 5 KX and (B) EDAX spectrum of synthesized TiO_2 composite
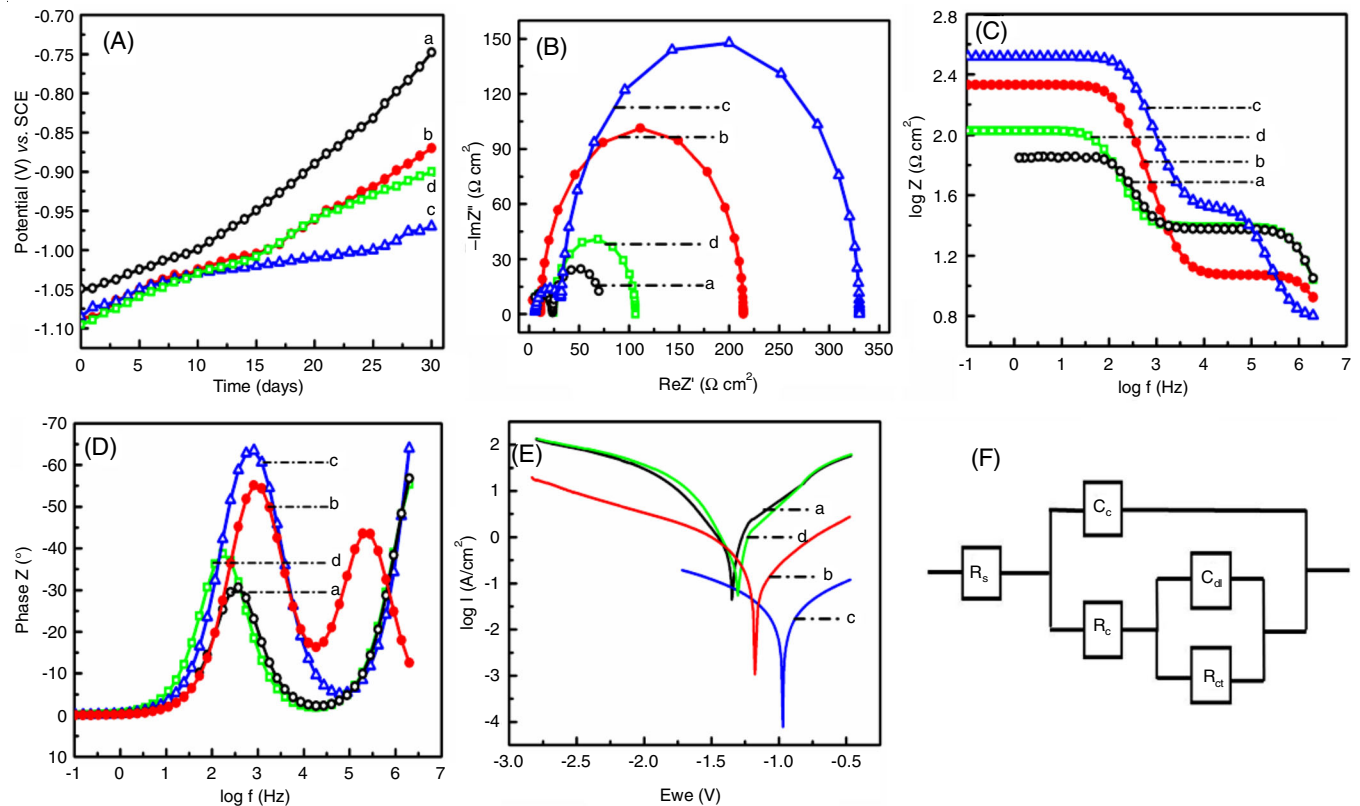
Fig. 3. (A) OCP decay curves, (B) Nyquist plots, (C) Bode impedance, (D) Bode phase and (E) Tafel plots and of hot-dip zinc coating in 3.5 wt.% NaCl solution; (a) pure zinc coating, (b) 0.1, (c) 0.2 and (d) 0.5 wt.% TiO$_2$ incorporated hot-dip zinc coating and (F) Equivalent circuit used for fitting the impedance data

drastic anodic shift in the range of -0.75 V to -0.80 V due to the faster dissolution of zinc from Fe-Zn intermetallic layers. The coatings incorporated with 0.2 wt.% nano TiO$_2$ composite exhibited least shift in their OCP values when compared with 0.1 wt.% and 0.5 wt.% nano TiO$_2$ incorporated hot-dip zinc coatings, revealing its best galvanic performance. This could be ascribed to the formation of a compact structure and an adherent protective layer as a result of optimum amount of nano TiO$_2$ incorporation. From the OCP analysis, it was understood that the corrosion resistance of hot-dip zinc coatings would be substantially improved by the incorporation of nano TiO$_2$ composite.

Electrochemical impedance analysis (EIS): The Nyquist plots obtained for pure and nano TiO$_2$ incorporated hot-dip zinc coatings in 3.5 wt.% NaCl solution are shown in Fig. 3B. The equivalent circuit used to fit the electrochemical impedance analysis is shown in Fig. 3F. It consisted of two intra- equivalent circuit which describes the diffusion-controlled process or inhibition characteristics. In this equivalent circuit, R$_s$ is the solution resistance, R$_c$ is the coating resistance, R$_{ct}$ is the charge transfer resistance, C$_c$ is the coating capacitance and C$_{dl}$ is the

double layer capacitance. These impedance parameters are compared in Table-1.

The impedance spectrum of pure zinc coating exhibited a depressed semicircular portion, meanwhile a well-defined semi-circle portion was observed in the case of nano TiO$_2$ incorporated coating. These semicircles have been connected with charge transfer resistance of the corrosion process and finite thickness layer diffusion process [24]. From the Nyquist plots, it was found that the diameter of the semi-circle was higher in the case of nano TiO$_2$ incorporated coating, which revealed its high charge transfer resistance R$_{ct}$. It was reported that the R$_{ct}$ value is reciprocally proportional to corrosion rate. So, the composite incorporated coating with high R$_{ct}$ value exhibited lower corrosion rate. The pure zinc coating exhibited higher corrosion rate due to its low R$_{ct}$ value. From the AC impedance analysis, it was confirmed that pure zinc coating had undergone severe corrosion. While a comparatively better performance was exhibited by nano TiO$_2$ incorporated coating. This revealed the existence of an effective barrier layer on the surface of composite incorporated coating. These results were found to be in accordance with other electrochemical test results.

TABLE-1
COMPARISON OF ELECTROCHEMICAL IMPEDANCE PARAMETERS OF PURE ZINC AND DIFFERENT
COMPOSITION OF TiO$_2$ NANOPARTICLE INCORPORATED HOT-DIP ZINC COATINGS

Coatings	R$_s$ (Ω cm^2)	R$_c$ (Ω cm^2)	C$_c$ (µF/cm^2)	R$_{ct}$ (Ω cm^2)	C$_{dl}$ (µF/cm^2)
Pure zinc	10.59	18.30	3.8×10^{-6}	27.39	2.8×10^{-6}
Zn + 0.1 wt.% TiO$_2$	18.29	25.31	2.7×10^{-6}	50.19	2.1×10^{-6}
Zn + 0.2 wt.% TiO$_2$	45.83	58.39	0.85×10^{-6}	180.72	0.91×10^{-6}
Zn + 0.5 wt.% TiO$_2$	32.62	27.63	1.9×10^{-6}	110.52	1.3×10^{-6}

The better performance of the optimized coating is also evident from the Bode impedance and phase angle plots (Fig 3C and 3D). The highest impedance values at low frequencies and higher phase angle values at high frequencies of 0.2 wt.% TiO_2 incorporated coating correspond to the formation of a highly corrosion-resistant and compact coating.

Potentiodynamic polarization studies: The pure and nano TiO_2 incorporated hot-dip zinc coatings were subjected to linear sweep voltammetric analysis and corresponding Tafel plots are shown in Fig 3E. The electrochemical Tafel parameters such as E_{corr}, I_{corr}, R_p and corrosion rate of hot-dip zinc coatings are shown in Table-2.

TABLE-2
COMPARISON OF ELECTROCHEMICAL
PARAMETERS OF TAFEL PLOTS OF PURE ZINC AND
DIFFERENT COMPOSITION TiO_2 NANOPARTICLE
INCORPORATED HOT-DIP ZINC COATINGS

Parameters	Coatings			
	Pure zinc	Zinc + 0.1 wt.% TiO_2	Zinc + 0.2 wt.% TiO_2	Zinc + 0.5 wt.% TiO_2
E_{corr} (V)	-1.36	-1.32	-0.97	-1.18
i_{corr} ($\mu A/cm^2$)	1.62×10^{-6}	0.91×10^{-6}	0.08×10^{-6}	0.35×10^{-6}
β_a (mV/dec)	436.78	445.92	440.29	430.31
β_c (mV/dec)	324.12	367.27	379.26	315.72
R_p (Ω cm^2)	49.86	96.10	2949.07	225.93
CR (mmpy)	3.58	2.71	0.93	1.75
IE (%)	–	43.83	95.06	78.40

The corrosion potential value (E_{corr}) of the optimized nano TiO_2 (0.2 wt.%) incorporated hot-dip zinc coating was found to be significantly high (-0.96 V) as that of pure zinc coating (-1.32 V). The acceleration of corrosion reaction and increase in E_{corr} value to more passive region was mainly due to the presence of nano TiO_2 in hot-dip zinc coating. A significantly low corrosion current density value (I_{corr}) was exhibited by nano TiO_2 incorporated hot-dip zinc coating (0.08×10^{-6} $\mu A/cm^2$) when compared with pure zinc coating (1.62×10^{-6} $\mu A/cm^2$). The polarization resistance (R_p) is inversely proportional to corrosion current density, which could be explained by the following equation:

$$R_p = \frac{\beta_a \beta_c}{2.303(\beta_a + \beta_c)\, i_{corr}}$$

where β_a and β_c are anodic and cathodic slopes. The R_p values of pure and nano TiO_2 incorporated hot-dip zinc coatings were calculated using the above equation. The optimized hot-dip coating exhibited a high R_p value of 2949.07 Ωcm^2 while it was found to be 49.86 Ωcm^2 in the case of pure zinc coating. It was well known that the R_p value is reciprocally proportional to corrosion rate. The corrosion rate values of hot-dip zinc coatings displayed in Table-2, which revealed the enhanced corrosion resistance of nano TiO_2 incorporated coating. From this study, it was concluded that the presence of 0.2 wt.% nano TiO_2 composite in the coating was the cause for the displacement of cathodic branch towards lower current densities, highest R_p value and highest E_{corr} values of the coating. As a result of this, the corrosion of hot-dip zinc coatings in aggressive environments could be suppressed effectively by adding 0.2 wt.% nano TiO_2 incorporation.

Effective incorporation of TiO_2 composite: The XRD patterns of pure and nano TiO_2 incorporated hot-dip zinc coatings in the 2θ range of 20-80º are shown in Fig. 4. In Fig. 4A, the strong peaks at 2θ = 43.7º, 54.9º and a weak peak at 71.2º are the characteristics of (101), (102) and (103) planes of metallic zinc (JCPDS 87-713) [25]. Most of the diffraction lines shown by diffractograms revealed the zinc hexagonal structure. The composite incorporated hot-dip zinc coating exhibited a similar diffraction pattern with diminished peaks, but the preferential orientation of the zinc matrix has been modified. Three additional peaks were observed in nano TiO_2 incorporated hot-dip zinc coating at 2θ values between 30º and 40º, indicating the presence of ZnO particles and anatase TiO_2 composite. The peaks at 2θ values 35.5º and 37.2º corresponds to (002) and (101) planes of ZnO (JCPDS 36-1451) and 38.7º corresponds to (004) plane of anatase TiO_2 (JCPDS 21-1272). The peak intensity of zinc at (102) plane was drastically reduced in the composite incorporated coating and peak at (103) plane was absent, indicating the effective incorporation of nano TiO_2 composite into the zinc matrix. The decreased peak intensities of composite incorporated coating, when com-
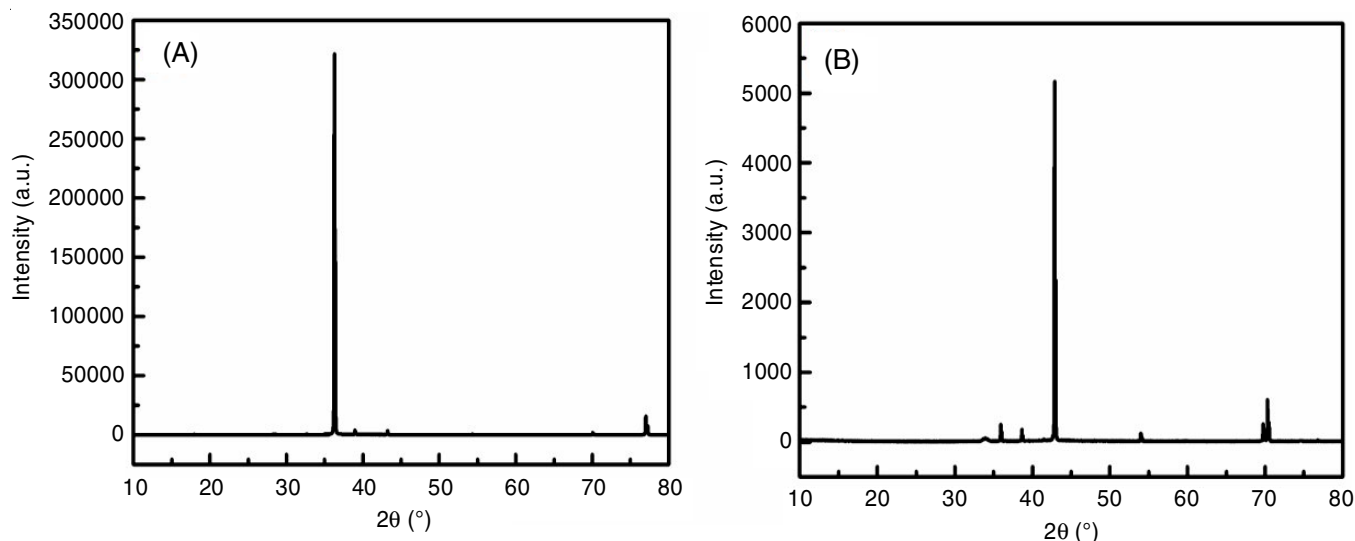
Fig. 4. XRD pattern of hot-dip zinc coating (A) pure zinc and (B) TiO_2 incorporated hot-dip zinc coating

pared with pure zinc coating suggested that the growth of crystals along this plane decreased due to the incorporation of TiO_2. The composite incorporated coating possessed peak width that was slightly broader than pure zinc coating due to the grain size reduction as a consequence of inert particle incorporation [26]. The presence of intense peaks in the XRD patterns indicated high crystallinity of the coatings. The EDAX analysis was also performed to confirm the effective incorporation of nano TiO_2 into zinc matrix.

Evaluation of improved surface morphology: The SEM images of pure and 0.2 wt.% nano TiO_2 incorporated hot-dip zinc coatings are shown in Fig. 5A$_1$ & 5A$_2$, respectively. The SEM images revealed the presence of spangles with larger size on the surface of nano TiO_2 incorporated coating. The micrographs of nano TiO_2 incorporated coating showed uniform grain size and the particles were uniformly distributed throughout the surface of the coating. The homogeneous defect free surface of nano TiO_2 incorporated zinc coating with well-defined grains was clear from the SEM images. The non-porous behaviour of optimum amount of composite incorporated coating may be due to the distribution of nano TiO_2 particles over the pores of zinc coating layers [27]. From the SEM images, it was concluded that nano TiO_2 incorporated hot-dip zinc coating had uniform coating structure with compact alloy layers.

Confirmation for the effective incorporation of TiO_2 composite: The effective incorporation of nano TiO_2 into zinc coating was confirmed on the basis of elemental composition of the hot-dip zinc coatings. The elemental composition of pure and nano TiO_2 incorporated hot-dip zinc coatings was examined based on EDAX spectra and are represented in Fig. 5B$_1$ & 5B$_2$. The elemental distribution corresponds to Fig. 5B$_1$ indicated that zinc and oxygen were the major elements in the case of pure zinc coating. But in the case of composite incorporated coating, the peaks correspond to zinc, titanium and oxygen was evident from the EDAX spectrum (Fig. 5B$_2$). The percentage composition of oxygen was found to be higher in the case of nano TiO_2 incorporated zinc coating. The presence of peak corresponds to titanium element when compared with pure zinc coating indicated the effective incorporation of nano TiO_2 into zinc matrix. These results were in good agreement with XRD results, which confirmed the effective incorporation of nano TiO_2 composite into hot-dip zinc coating. The presence of titanium and increment in the percentage composition of oxygen in the EDAX spectrum also revealed the role of TiO_2 composite for the structural modification of outer layer of pure zinc coating.

Enrichment of different intermetallic layers

Identification of dissolution of different phases: The hot-dip zinc coatings were subjected to anodic dissolution in 3.5 wt.% NaCl solution by applying a current density of 10 mA/cm^2 for 1 h. Variation of potential of different layers with
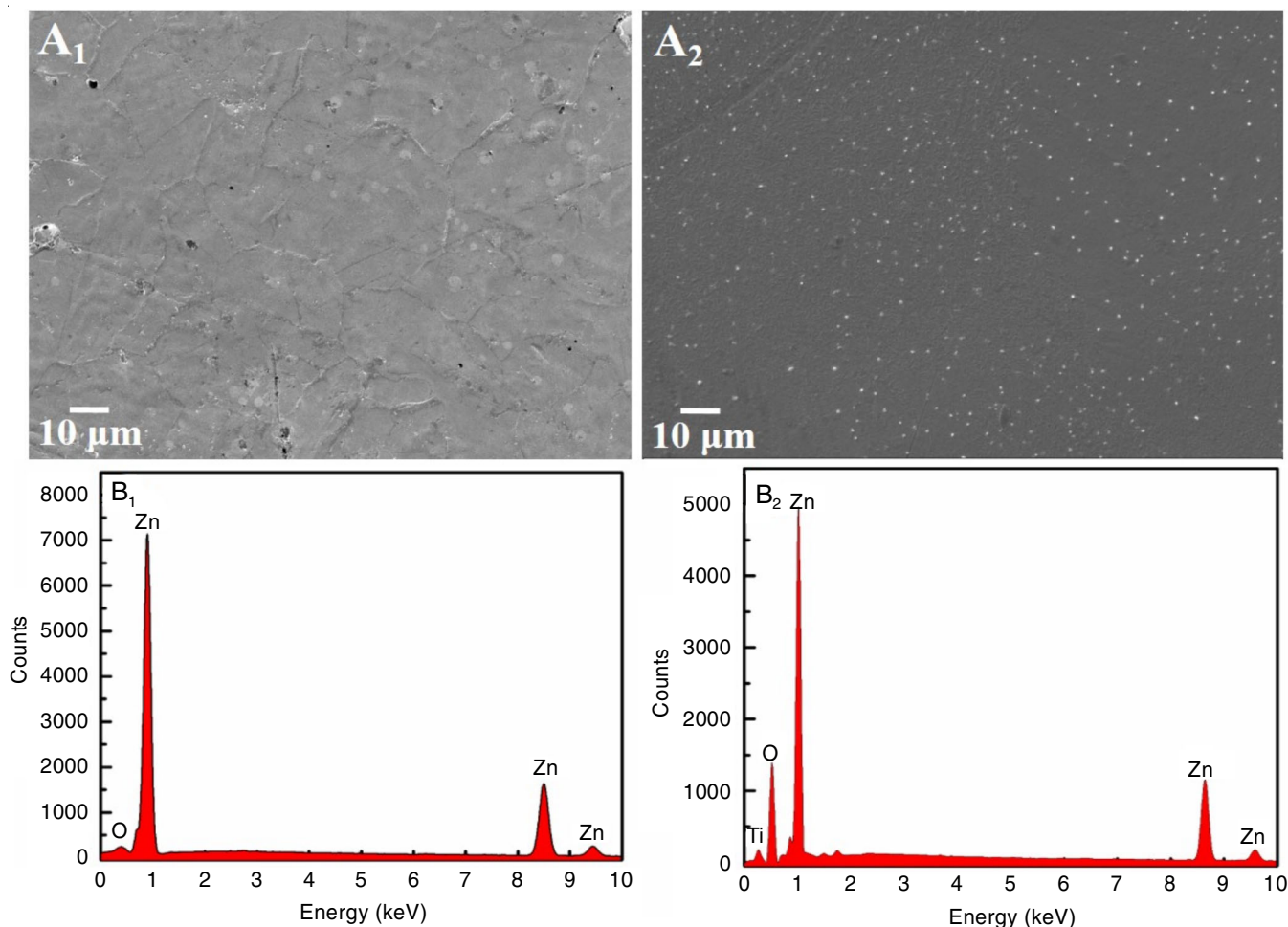
Fig. 5. SEM images and EDAX spectrum of (A$_1$) & (B$_1$) pure zinc and (A$_2$) & (B$_2$) TiO_2 incorporated hot-dip zinc coatings, respectively

TABLE-3
IMPEDANCE PARAMETERS OF EQUIVALENT CIRCUITS OF DIFFERENT INTERMETALLIC LAYERS OF
TiO₂ NANOPARTICLE INCORPORATED HOT-DIP ZINC COATING AT EACH STAGE OF ANODIC
DISSOLUTION AT 10 mA/cm², OBTAINED AFTER Z FITTING OF NYQUIST PLOTS

Coatings	R_s (Ω cm²)	R_c (Ω cm²)	C_c (μF/cm²)	R_{ct} (Ω cm²)	C_{dl} (μF/cm²)
Before dissolution	45.83	58.39	0.85×10^{-6}	180.72	0.91×10^{-6}
After 0.50 h dissolution	28.49	32.65	1.48×10^{-6}	83.10	1.85×10^{-6}
After 0.75 h dissolution	17.49	27.12	1.83×10^{-6}	5.81	2.41×10^{-6}

respect to extent of dissolution was monitored and shown in Fig. 6. The more negative potential during the early stage of anodic dissolution indicated the presence of outermost pure zinc layer. This layer dissolved out easily due to the sacrificial nature of zinc top layer leading to exposure of inner alloy layers.
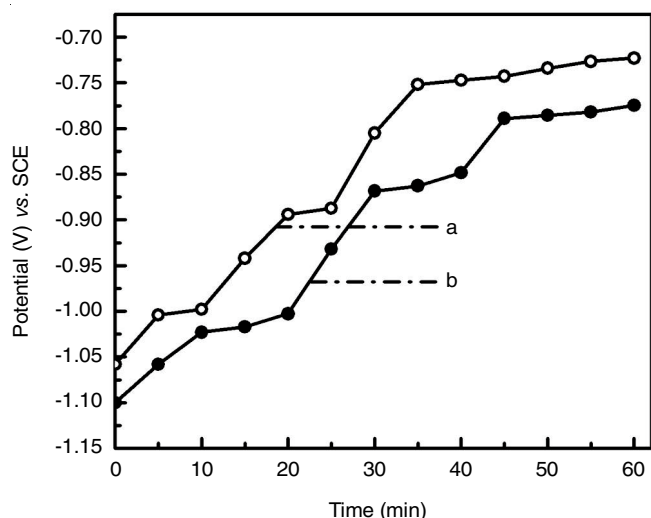
Fig. 6. Potential vs time curve of (a) Pure zinc hot-dip zinc coating and (b) TiO₂ composite incorporated hot-dip zinc coating at a current density of 10 mA/cm²

In case of the pure zinc coating, the inter metallic layers dissolved out completely within 24 min of anodic dissolution compared with 0.2 wt.% nano TiO₂ incorporated coating, where the complete dissolution took place within 28 min only. This revealed the better galvanic performance of composite incorporated coating. In Fig. 6, each plateau represents each inter metallic layers, where the potential remains constant. The exposed layer consists of more iron content having more positive potential and optimum zinc content having more negative potential. The slower dissolution of Fe-Zn intermetallic layers could be attributed to the better diffusion of zinc and the composite in to mild steel substrate during hot-dip galvanization, which resulted in the formation of compact alloy layers.

Electrochemical evaluation of different Fe-Zn intermetallic layers

Electrochemical impedance analysis: Electrochemical impedance spectroscopic analysis of different intermetallic layers after anodic dissolution at different time periods was carried out to get a clear idea about the electrochemical characteristics, corresponding Nyquist plots are shown in Fig. 7A. The equivalent circuit used to fit the electrochemical impedance analysis is shown in Fig. 7E and the electrochemical impedance parameters are shown in Table-3.

From the Nyquist plots, the diameter of semi-circle was higher in the case of ETA layer and having high charge transfer resistance and polarization resistance, revealed the ETA layer with high R_p value exhibited lower corrosion rate. From this study, it is concluded that the nano TiO₂ incorporated coating showed better galvanic performance than pure zinc coating and also ETA layer having the electrochemical stability and galvanic performance than other Fe- Zn intermetallic layers. This was due to the inhibiting action of nano TiO₂ concentration, which is high in the eta layer than other layers, which leads to enhanced corrosion resistance.

Bode impedance and phase angle plots of different intermetallic layers after anodic dissolution are shown in Fig. 7B and 7C, respectively. High impedance and phase angle values revealed the enhanced corrosion prevention characteristics of η layer.

Potentiodynamic polarization studies: Tafel polarization behaviour of different intermetallic layers after anodic dissolution at different time periods is shown in Fig. 7D. The electrochemical Tafel parameters such as corrosion potential, corrosion current density, anodic slope, cathodic slope and polarization resistance of galvannealed coatings are given in Table-4. The η phase exhibits comparatively lower corrosion current density $(0.08 \times 10^{-6} \mu$A/cm²) and corrosion rate (0.93 mmpy) than other intermetallic layers. The reduction in corrosion current density revealed anti-corrosion characteristics of the η phase. The effective incorporation of TiO₂ into the coating reduces active sites favourable for corrosion and makes the coating more compact and corrosion resistant. High corrosion prevention characteristics of η phase were due to the high percentage composition of TiO₂. Role of Fe-Zn intermetallic alloy layer has to be taken into the consideration while describing the long-term performance of galvanized steel.

TABLE-4
TAFEL PARAMETERS OBTAINED FOR TiO₂ NANOPARTICLE
INCORPORATED HOT-DIP ZINC COATING AT EACH
STAGE OF ANODIC DISSOLUTION AT 10 mA/cm²

| Parameters | Coatings | | |
	Before dissolution	After 0.50 h dissolution	After 0.75 h dissolution
E_{corr} (V)	-0.97	-1.08	-1.17
i_{corr} (μA/cm²)	0.08×10^{-6}	0.11×10^{-6}	0.20×10^{-6}
β_a (mV/dec)	440.29	380.45	342.92
β_c (mV/dec)	379.26	310.19	299.31
R_p (Ω cm²)	2949.07	927.45	346.98
CR (mmpy)	0.93	1.28	1.85

Conclusion

Anatase TiO₂ incorporated hot-dip zinc coatings with defect free nanostructured surface morphology was developed
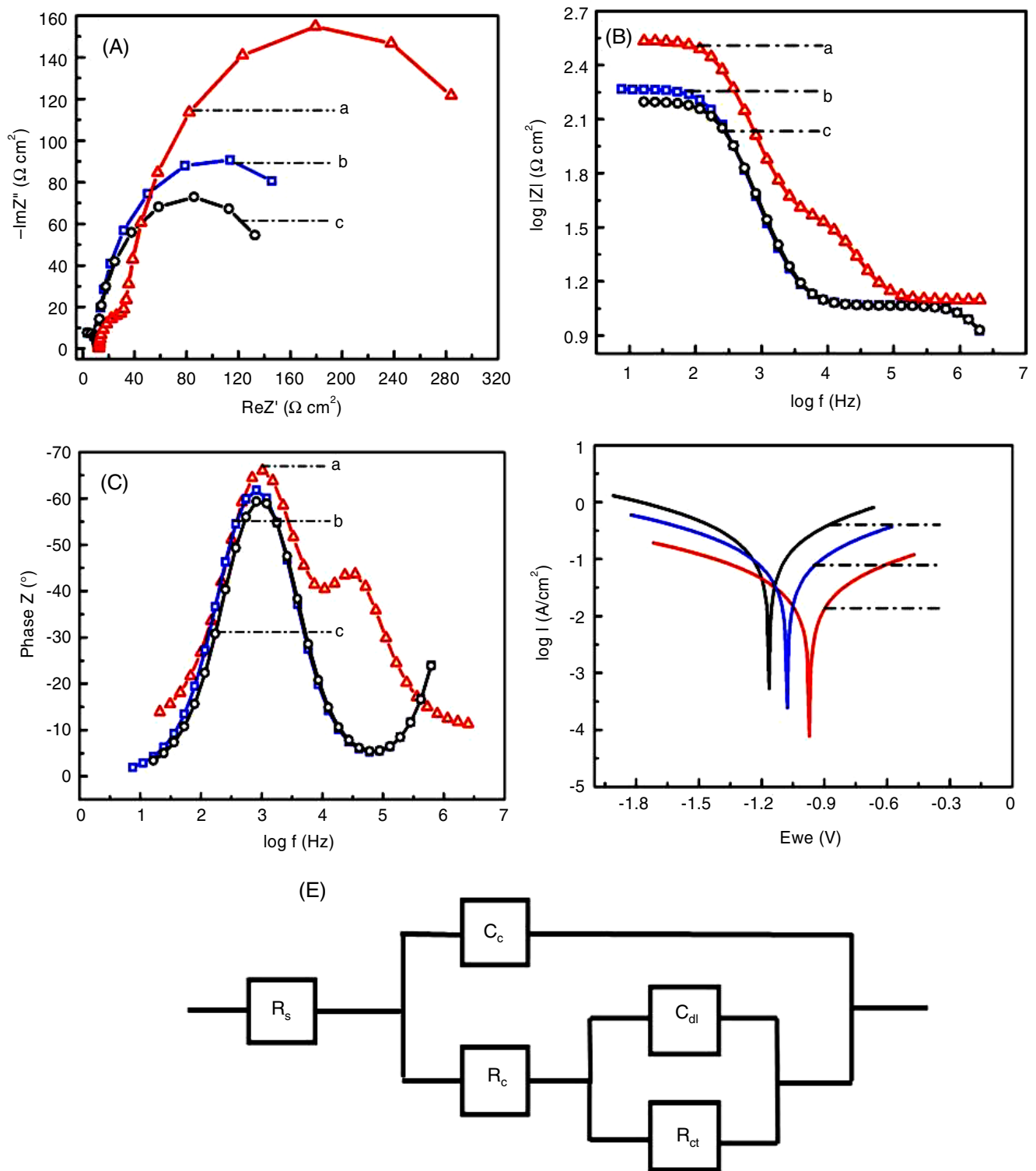
Fig. 7. (A) Nyquist plot, (B) Bode plot, and (C) Bode phase diagram, (D) Tafel polarization curve of TiO$_2$ composite incorporated hot-dip zinc coating at each stage of anodic dissolution at 10 mA/cm^2; (a) before dissolution (b) after 0.50 h and (c) after 0.75 h and (E) Equivalent circuit used for fitting the impedance data

successfully for the corrosion protection of steel. The improved surface morphology of nano TiO$_2$ incorporated hot-dip zinc coatings leads to enhancement in galvanic performance and corrosion resistant properties of hot-dip zinc coatings under aggressive conditions. The developed coatings exhibited low corrosion current density and high polarization resistance com-

pared with pure zinc coating, attributed to the enhanced corrosion resistance of nano TiO$_2$ incorporated hot-dip zinc coatings. The layer-wise dissolution characteristics of the coatings revealed the compact inner alloy structure and stability of Fe-Zn intermetallic layers.

ACKNOWLEDGEMENTS

CONFLICT OF INTEREST

The authors declare that there is no conflict of interests regarding the publication of this article.

REFERENCES

1. A. Gallego, J.F. Gil, E. Castro and R. Piotrkowski, *Surf. Coat. Technol.*, **201**, 4743 (2007);
   https://doi.org/10.1016/j.surfcoat.2006.10.018
2. S.M.A. Shibli and R. Manu, *Surf. Coat. Technol.*, **197**, 103 (2005);
   https://doi.org/10.1016/j.surfcoat.2004.10.115
3. M. Dutta, A.K. Halder and S.B. Singh, *Surf. Coat. Technol.*, **205**, 2578 (2010);
   https://doi.org/10.1016/j.surfcoat.2010.10.006
4. C.D. Lokhande, S.K. Min, K.D. Jung and O.S. Joo, *J. Mater. Sci.*, **39**, 6607 (2004);
   https://doi.org/10.1023/B:JMSC.0000044903.93296.a4
5. S.M.A. Shibli, V.S. Dilimon, S.P. Antony and R. Manu, *Surf. Coat. Technol.*, **200**, 4791 (2006);
   https://doi.org/10.1016/j.surfcoat.2005.04.058
6. H. Shi, F. Liu, E. Han and Y. Wei, *J. Mater. Sci. Technol.*, **23**, 551 (2007).
7. S.K. Dhoke and A.S. Khanna, *Corros. Sci.*, **51**, 6 (2009);
   https://doi.org/10.1016/j.corsci.2008.09.028
8. S.K. Dhoke and A.S. Khanna, *J. Appl. Polym.*, **113**, 2232 (2009);
   https://doi.org/10.1002/app.30276
9. S.K. Dhoke, A.S. Khanna and T.J.M. Sinha, *Prog. Org. Coat.*, **64**, 371 (2009);
   https://doi.org/10.1016/j.porgcoat.2008.07.023
10. S.M.A. Shibli and F. Chacko, *Surf. Coat. Technol.*, **205**, 2931 (2011);
    https://doi.org/10.1016/j.surfcoat.2010.10.067
11. T. Sreethawong, Y. Suzuki and S. Yoshikawa, *J. Solid State Chem.*, **178**, 329 (2005);
    https://doi.org/10.1016/j.jssc.2004.11.014
12. W. Su, J. Zhang, Z. Feng, T. Chen, P. Ying and C. Li, *J. Phys. Chem. C*, **112**, 7710 (2008);
    https://doi.org/10.1021/jp7118422
13. C.H. Sun, X.H. Yang, J.S. Chen, Z. Li, X.W. Lou, C. Li, S.C. Smith, G.Q. Lu and H.G. Yang, *Chem. Commun.*, **46**, 6129 (2010);
    https://doi.org/10.1039/c0cc00832j
14. S. Perumal, C.G. Sambandam, K.M. Prabu and S. Ananthakumar, *Int. J. Res. Eng. Technol.*, **3**, 651 (2014).
15. H.G. Yang, C.H. Sun, S.Z. Qiao, J. Zou, G. Liu, S.C. Smith, H.M. Cheng and G.Q. Lu, *Nature*, **453**, 638 (2008);
    https://doi.org/10.1038/nature06964
16. Y. Sohn, *Appl. Surf. Sci.*, **257**, 1692 (2010);
    https://doi.org/10.1016/j.apsusc.2010.08.124
17. T.R. Aju Thara, P.P. Rao, S. Divya, A.K. Raj and T.S. Sreena, *ACS Sustain. Chem. Eng.*, **5**, 5118 (2017);
    https://doi.org/10.1021/acssuschemeng.7b00485
18. S. Ghasemi, S. Rahimnejad, S.R. Setayesh, S. Rohani and M.R. Gholami, *J. Hazard. Mater.*, **172**, 1573 (2009);
    https://doi.org/10.1016/j.jhazmat.2009.08.029
19. W.C. Hung, Y.C. Chen, H. Chu and T.K. Tseng, *Appl. Surf. Sci.*, **255**, 2205 (2008);
    https://doi.org/10.1016/j.apsusc.2008.07.079
20. K.I. Liu, Y.C. Hsueh, H.S. Chen and T.P. Perng, *J. Mater. Chem. A Mater. Energy Sustain.*, **2**, 5387 (2014);
    https://doi.org/10.1039/c3ta15007k
21. R. Nandanwar, P. Singh, F.F. Syed and F.Z. Haque, *Orient. J. Chem.*, **30**, 1577 (2014);
    https://doi.org/10.13005/ojc/300417
22. 22 B. Erdem, R.A. Hunsicker, G.W. Simmons, E.D. Sudol, V.L. Dimonie and M.S. El-Aasser, *Langmuir*, **17**, 2664 (2001);
    https://doi.org/10.1021/la0015213
23. X. Zhang, M. Zhou and L. Lei, *Carbon*, **43**, 1700 (2005);
    https://doi.org/10.1016/j.carbon.2005.02.013
24. V. Barranco, S. Feliu Jr. and S. Feliu, *Corros. Sci.*, **46**, 2203 (2004);
    https://doi.org/10.1016/j.corsci.2003.09.032
25. L. Shi, K. Bao, J. Cao and Y. Qian, *CrystEngComm*, **11**, 2308 (2009);
    https://doi.org/10.1039/b909599c
26. K. Vathsala and T.V. Venkatesha, *Appl. Surf. Sci.*, **257**, 8929 (2011);
    https://doi.org/10.1016/j.apsusc.2011.05.067
27. S.M.A. Shibli, F. Chacko and C. Divya, *Corros. Sci.*, **52**, 518 (2010);
    https://doi.org/10.1016/j.corsci.2009.10.008